Large kinetic asymmetry in the metal-insulator transition nucleated at localized and extended defects

W. Fan, J. Cao, J. Seidel, Y. Gu, J. W. Yim, C. Barrett, K. M. Yu, J. Ji, R. Ramesh, L. Q. Chen, and J. Wu

Phys. Rev. B **83**, 235102 — Published 2 June 2011

DOI: 10.1103/PhysRevB.83.235102

Large Kinetic Asymmetry in Metal-Insulator Transition Nucleated at Localized and Extended Defects

W. Fan[1, 2], J. Cao[1, 3], J. Seidel[3], Y. Gu[4], J. W. Yim[1, 3], C. Barrett[1,3], K. M. Yu[3], J. Ji[2], R. Ramesh[1,3], L. Q. Chen[4], J. Wu[1,3, #]

1. Department of Materials Science and Engineering, University of California, Berkeley, Berkeley, California 94720, USA

2. Department of Thermal Science and Energy Engineering, University of Science and Technology of China, Hefei, China

3. Materials Sciences Division, Lawrence Berkeley National Laboratory, Berkeley, California 94720, USA

4. Department of Materials Science and Engineering, Pennsylvania State University, University Park, Pennsylvania 16802, USA

To whom correspondence should be addressed: wuj@berkeley.edu

PACS numbers: 71.30.+h, 72.20.-i, 72.80.Ga

ABSTRACT

Superheating and supercooling effects are characteristic kinetic processes in first-order phase transitions, and asymmetry between them is widely observed. In materials where electronic and structural degrees of freedom are coupled, a wide, asymmetric hysteresis may occur in the transition between electronic phases. Structural defects are known to seed heterogeneous nucleation of the phase transition, hence reduce the degree of superheating and supercooling. Here we show that in the metal-insulator transition of single-crystal VO_2, a large kinetic asymmetry arises from the distinct spatial extension and distribution of two basic types of crystal defects: point defects and twin walls. Nanometer-thick twin walls are constantly consumed but re-generated during the transition to the metal phase, serving as dynamical heterogeneous nucleation seeds and eliminating superheating; On the other hand, the transition back to the insulator phase relies on nucleation at point defects because twinning is structurally forbidden in the metal phase, leading to a large supercooling. By controlling the formation, location and extinction of these defects, the kinetics of the phase transition might be externally modulated, offering possible routes toward new memory and logic device technologies.

I. INTRODUCTION

Supersaturation is a kinetic phenomenon frequently observed in first-order phase transitions, in which the low-temperature phase persists above the transition temperature (superheating) and the high-temperature phase persists below the transition temperature (supercooling). The degree of superheating is not necessarily equal to that of the supercooling. For example, a large asymmetry exists in melting / crystallization of elemental metals [1] and water [2]. Asymmetric phase transitions also arise in correlated electron materials where electronic and structural degrees of freedom are coupled, such as asymmetric hysteresis in electric conductivity in VO_2 [3, 4] and $NdNiO_3$ [5], and magnetization in $Ce(FeRu)_2$ [6, 7] and $CuMoO_4$ [8], but the microscopic origin remains elusive. Defects are known to seed heterogeneous nucleation of the structural phase transition, hence reduce the degree of superheating or supercooling. Here we show that a large kinetic asymmetry may arise from the distinct spatial extension and distribution of two basic types of crystal defects: point defects and twin walls. In the structural transition, the low-symmetry structure mimics higher-symmetry structure at its twin wall [9]. We show that such a twin wall can act as a catalyst to *dynamically* and *sustainably* nucleate the high-symmetry structure during the transition; in contrast, the transition back to the low-symmetry structure relies on nucleation at point defects. The distinct topology and distribution of twin wall and point defects result in disordered nucleation and coexistence of electronic phases during heating, but long-range phase ordering during cooling.

Our investigation of the large kinetic asymmetry is based on probing the model metal-insulator phase transition (MIT) kinetics in twinned and twin-free single-crystal vanadium dioxide (VO_2) microbeams (MBs). Twin walls of the insulator phase in VO_2

micro-platelets have recently been discovered to undergo a MIT separately from the bulk [10, 11]. The geometry and lattice orientation of our MBs restrict the two phases to coexist one dimensionally along the MB axis [12]. This eliminates the percolation process in MIT in thin films [13] or frustrated domain structures in platelets [10], allowing its initial nucleation process to be directly, electrically probed. Strain-free VO_2 undergoes the first-order MIT at $T_C^0 \approx 68^oC$ with a drastic change in conductivity and optical reflection [14-16]. The MIT is accompanied with a structural change from the low-temperature, insulating, monoclinic phase (M) to the high-temperature, metallic, tetragonal phase (rutile structure, R) [14]. It is known that another monoclinic, insulating structure (M_2, differentiated from the first M phase known as M_1) can be induced by uniaxial compression perpendicular to c_R [14, 15, 17] or uniaxial tension parallel to c_R [18, 19]. The transition from M_1 to R features a spontaneous strain of -1% (shrinkage along the c_R direction), while the spontaneous strain is 0.3% (elongation along c_R) across the M_1 to M_2 transition [15]. Consequently, according to the Clapeyron equation, uniaxial compression (or tension) along c_R drives the M_1 structure toward the R (or M_2) structure [20]. It is established that under white-light illumination, both M_1 and M_2 phases of VO_2 show a brighter optical reflectivity than the R phase [12]. This provides a convenient way to identify the phase transition temperature and to image the M/R domain structure.

II. EXPERIMENTAL DETAILS

VO_2 MBs were prepared using the vapor transport method reported previously. [21] During the high temperature synthesis (~980 ^oC), these MBs crystallize along the c_R direction with $\{110\}_R$ planes as bounding facets on a molten SiO_2 surface. When cooled to lower temperatures, the SiO_2 surface gradually solidifies, mechanically clamping the

VO_2 MBs onto the SiO_2 surface. A small percentage of these MBs grow out of the edge of the Si wafer forming long cantilevers, allowing investigation of the MIT in strain-free MBs. For electrical measurement, metal electrodes (15 nm Cr and 400 nm Au) were patterned using standard photolithography and deposited with electron beam evaporation.

Additional bulk point defects were introduced by 3 MeV α particles irradiation with controlled doses ($0.01 \sim 2 \times 10^{16}$ cm^{-2}). The irradiation was performed using a 2.13 MeV He^{2+} beam with current between 40 and 150 nA generated by a Pelletron tandem accelerator. The ion beam was defocused to an area of 40 mm^2 to cover the entire sample. Simulations using the stopping and range of ions in matter (SRIM) software predicted that the concentration of defects generated by the ion beam is relatively uniform, and the ions would penetrate the entire thickness of the VO_2 layer, leaving end of range damage in the substrate. Electrical and optical measurements were carried out right after each irradiation experiments to minimize possible aging effects.

III. RESULTS AND DISCUSSION

(a) Experimental Results

Figure 1 (a) shows the temperature (T) dependence of four-probe resistance (R_{MB}) of two types of MB devices: free-standing and substrate-clamped. The free-standing devices were fabricated with VO_2 MBs suspended from the substrate [12]. Its R_{MB} shows an abrupt, single jump down at T_{heat} upon heating and another abrupt jump up at T_{cool} upon cooling, consistent with abrupt change in optical reflection in free-standing MBs. The superheating and supercooling behavior is symmetric, and the hysteresis width between T_{heat} and T_{cool} is ~ 13°C in these MBs. The clamped devices, in stark contrast, feature

wide and asymmetric M → R and R → M transitions. The temperature at which R_{MB} finally drops to the R-phase level is raised from T_C^0 to ~ 97 °C. This shift in T_C is expected as the clamping induces uniaxial tensile strain along the MBs [18]. What is striking is the *gradual, continuous* decrease in R_{MB} during heating contrasted to the *sudden*, *large* jump up in R_{MB} during cooling. This drastically asymmetric heating-cooling behavior in clamped VO_2 MBs is consistent with observations from several other groups [4, 12], but no explanations were given. During heating, R_{MB} initially follows an Arrhenius temperature dependence ($R_{MB} \propto \exp(E_a/k_BT)$) in the M phase, with E_a ~ 0.3eV, consistent with previously reported data [4, 22]. At $T_1 \approx 62$ °C, R_{MB} starts to decrease more rapidly deviating from the Arrhenius dependence, characterized by small steps jumping downward (Fig.1(b) inset). This deviation signifies the emergence of the first R domains that reduce the total resistance. As will be shown later, these first R domains always nucleate around the twin walls of the M_1 phase. Unlike in thin films, in the MB geometry these domains span the entire width of the MB and line up one-dimensionally along the MB [12]. Therefore, the total MB resistance R_{MB} sensitively reveals the nucleation process of these R domains. Around $T_2 \approx 66$ °C, R_{MB} jumps up slightly, and then continues to decrease gradually until a high temperature T_3 (≈ 97 °C) where the entire MB becomes metallic R phase. The upward jump near T_2 is due to the emergence of domains of M_2 phase that is three times more resistive than the original M_1 phase [20]. These M_2 domains are induced because when the R domains grow sufficiently long, they impose a strong tensile strain to neighboring M_1 phase along the nanobeam axis direction (c_R), elastically driving it into the M_2 phase. But immediately after that, further increase in temperature causes more M_1 → R and M_2 → R transitions, resulting in monotonic and

continuous decrease in total R_{MB} until T_3. The smooth R_{MB} - T curve during heating indicates small or no superheating for the M $\rightarrow$ R transition. In contrast, the large supercooling in the R $\rightarrow$ M transition indicates that the transition is retarded and limited by nucleation of the M phase.

Numerous mini-steps exist on the heating R_{MB} - T curve between T_2 and T_3. These steps come from growth of the small R domains and reflect the M/R domain wall pinning and depinning process along the MB axial direction, akin to the Barkhausen avalanche associated with magnetic domain growth during magnetization. In percolative VO_2 thin films, the distribution of these steps was quantitatively investigated and self-organized criticality was suggested to explain the behavior [23]. We find that in clamped VO_2 MBs which are effectively an one-dimensional system for the domain dynamics, these mini-steps distribute as a broad peak (Peak A) between ~100 and 1000 Ω as shown in Fig.1(b). The larger R_{MB} steps between T_1 and T_2 distribute as another peak (Peak B) around ~ 20kΩ, distinctly isolated from the Peak A. The extremely large jumps during cooling are represented with a distinct peak (Peak C) on the ΔR_{MB} distribution, as shown in Fig.1(b). The isolated distribution of these three peaks reflects that distinct processes are responsible for these ΔR_{MB} steps.

To elucidate the domain nucleation and expansion process, Fig.2(a) shows optically imaged domain structure at selected temperatures, which leads to the following conclusions: i) during heating, the first R domains nucleate at $T_1 \approx 63^{o}$C at seemingly random positions; ii) at higher T, the randomly distributed R domains start to redistribute correlatively and order themselves; iii) the random R domain edges make an angle of either $\sim\pm65^{o}$ or 90^{o} to c_R, but when the R domains are ordered the angle is always 90^{o};

and most importantly, iv) during heating the expansion of R domains is smooth and gradual, yet during cooling the M domains emerge abruptly at periodic positions. It has been shown that the one-dimensionally ordered M/R domain structure is caused by energy minimization of the coherently strained MB/SiO_2 system [12, 24], where the domain period is determined by a competition between long-range elastic interaction with the SiO_2 surface and the positive M/R domain wall energy. Therefore, the random or ordered distribution of M/R domains signifies a short-range or long-range interaction, respectively, that governs the energetics of domain formation in the system. In the homogeneous nucleation theory, the energy barrier in the MIT of VO_2 is estimated to be ~ 600 eV [25] based on the M/R domain wall energy [12] and the transition latent heat (~ 5kJ/mol [20, 26]); therefore a homogeneous nucleation is not possible. Hence in both the M $\rightarrow$ R and R $\rightarrow$ M transitions the new phase must nucleate at special sites where the energy barrier is significantly reduced. The long-range interaction is the elastic coupling between the MB and the underneath SiO_2 surface with a characteristic length of the MB thickness (~μm) [24]. Therefore, the nucleation sites in the M $\rightarrow$ R transition must distribute with a mean distance comparable to or larger than ~ μm so that they appear random, whereas in the R $\rightarrow$ M transition much smaller than ~ μm so that they are statistically uniform. In the following we show that in the M $\rightarrow$ R transition upon heating, the nucleation sites are the M-phase twin walls. On the other hand, upon cooling the R $\rightarrow$ M transition nucleates at bulk point defects, because the higher-symmetry, R-phase structure forbids twinning. The point defects have high density but are not as effective as the twin walls in reducing the homogeneous nucleation barrier. Hence the kinetic

asymmetry in the MIT is an intrinsic effect and microscopically originates from the crystal structural asymmetry.

(b) Modulating Density of Point Defects

We first explore the role of bulk point defects in the MIT by modulating its density. This was achieved by irradiation with high-energy α particles at controlled doses, a standard method to introduce bulk point defects in semiconductors [27]. We find that in free-standing MBs, the transition temperature T_{heat} is reduced and T_{cool} is nearly symmetrically increased by the irradiation, as shown in Fig.2(b). In the clamped MBs, in contrast, at irradiation doses that would greatly reduce supersaturation of free-standing MBs, the R_{MB}-T dependence in the heating half-cycle remains essentially the same; but the supercooling in the cooling half-cycle is clearly reduced by the irradiation (Fig.2(c)). Monte Carlo modeling showed that irradiation with 3MeV α particles at a dose of 10^{16} cm^{-2} would generate native point defects (both vanadium and oxygen vacancies and interstitials) at a density of ~ 10^{20} cm^{-3}. The α particles all completely penetrate through the μm-thick VO_2 and only leave these point defects as damage in the MBs. The fact that T_{heat} and T_{cool} behave nearly symmetrically suggests that the nucleation barrier in the free-standing MBs is comparable for the R → M and M → R transitions, and bulk point defects play quantitatively the same role in reducing the barrier in both transition directions.

(c) Effects of Twin Walls

Next we investigate the role of twin walls in the MIT. It has been established that both the M_1 [11] and M_2 [20] phases are easily twinned under strain due to small energy

penalty of the twin walls and large energy benefit from strain relaxation. In MBs stretched along the axial c_R direction, micro x-ray diffraction (μ-XRD) [20] and μ-Raman [28] show that the MBs are in the M_2 phase and are twinned. In this geometry, only 180° M_2 twin walls are stable, with wall planes in $\{100\}_R$ or $\{010\}_R$ (i.e., $\{001\}_{M2}$ or $\{100\}_{M2}$), as shown in Fig.3(a) and (c). On the other hand, in axially compressed MBs the M_1 twin walls may form with two possible orientations [11]. The 180° M_1 twin walls lie in the plane of $\{001\}_R$ (i.e., $\{\bar{2}01\}_{M1}$) perpendicular to c_R, as shown in Fig.3(a) and (b), and the 90° M_1 twin walls lie in the plane of $\{112\}_R$ (i.e., $\{\bar{4}\,\bar{1}\,3\}_{M1}$) making an angle of ~ 66° with c_R. We find that at room temperature, free-standing MBs are always in un-twinned M_1 phase and the substrate clamping mostly causes M_1 twinning. The M_1 twin walls are perpendicular to the MB axis from the top view, and distributed sparsely along the MB. Figure 4(a) shows these M_1 twins imaged with polarized light reflection. The contrast could be due to either 180° or 90° M_1 twins, which the top-view polarized optical microscope cannot differentiate [11]. At higher temperatures, twinned M_2 phase appears with M_2 twin walls parallel to the MB axis and densely packed at a period of ~ 120 nm, as imaged with SEM in Fig.4(b) and identified with μ-XRD [20]. Considering that the M_2 phase is favored at tensile strain along c_M [20], we conclude that high tensile axial strain is developed at higher temperatures ($T > \sim T_2$).

It is interesting to note that the first R domains always nucleate around the M_1-phase twin walls, as shown in Fig.4(a). The random distribution of these twin walls along the MB results in an irregular and sparse pattern of the initial R domains. Upon further increase in T, these R domains grow *gradually* and *continuously* along c_R. During this process these R domains re-organize their locations and sizes, and become periodic when

the long-range elastic interaction starts to dominate over the short-range domain nucleation. During the cooling process, the first M domains appear *suddenly* at *periodic* positions but only after a large supercooling. It should be noted that the initial M_1 twin walls are localized and completely consumed after the nucleation of first R domains, but the M_2 twin walls are constantly generated during heating. Further growth of the R domains is mediated by M_2 twin walls in the neighboring region, which were induced by tensile strain created by the growth of R domains themselves. A self-sustained M $\rightarrow$ R transition process is thus established, nucleated initially at M_1 twin walls but thereafter mediated *dynamically* by M_2 twin walls. We show formation of such a complicated M_1/M_2/R domain structure in Fig.4(c) imaged by atomic force microscope (AFM), where the different phases can be distinguished by their height and domain periodicity. This is also consistent with the upward jump prior to T_2 in the R_{MB} - T curve in these devices (Fig.1(a)).

(d) Landau Theory and Phase Field Modeling

The R domains always nucleate out of the M-phase twin walls (either M_1 or M_2). This is because at the twin walls of the M phases, the crystal structure symmetry is locally elevated and thus mimics structurally the high-symmetry R phase [9]. In the simplest Ginzburg-Landau theory of first-order ferroelastic phase transition, the free energy can be written as a functional of the order parameter Q [9],

$$F(Q) = \frac{\alpha}{2}Q^2 + \frac{b}{4}Q^4 + \frac{c}{6}Q^6 + \frac{g}{2}(\nabla Q)^2, \qquad (1)$$

where $\alpha(T) = a \cdot (T - T_c)$, $a > 0$, $b < 0$, $c > 0$, and $g > 0$. Across a twin wall at $x = 0$, the well-known solution for Q is obtained by minimizing F [29],

$$Q(x) = Q_\infty \cdot \frac{\sinh(x/w)}{\sqrt{A + \sinh^2(x/w)}}, \quad (2)$$

where $w = \sqrt{g} \Big/ \left(Q_\infty \sqrt{cQ_\infty^2 + b/2}\right)$ is the wall width, and $A = \left(6cQ_\infty^2 + 3b\right) \Big/ \left(4cQ_\infty^2 + 3b\right)$. Q varies from $-Q_\infty$ at $x = -\infty$ to Q_∞ at $x = +\infty$, and vanishes at the wall (x = 0). It can be seen that the high-symmetry, paraelastic phase, which is characterized by Q = 0, is locally stabilized at the domain wall within a small range of $|x| <\sim w$.

The transformation strain along the longitudinal direction in the VO_2 MBs is tensile, while along the width direction is compressive. Therefore, when long-range MB-substrate clamping starts to dominate, domain edge rotation along with domain ordering is energetically favored. To fully simulate the domain structure evolution, a three-dimensional phase field model is necessary. We used a 2-4-6 Landau polynomial to describe the bulk free energy, where the two M_1 variants were described by the two order parameters, Q_1 and Q_2,

$$F(Q_1, Q_2) = \int_V \left[f(Q_1, Q_2) + \sum_{n=1,2} \frac{\kappa}{2} (\nabla Q_n)^2 + \frac{1}{2} C_{ijkl} (\varepsilon_{ij} - \sum_{n=1,2} Q_n^2 \varepsilon_{ij}^{0n})(\varepsilon_{kl} - \sum_{n=1,2} Q_n^2 \varepsilon_{kl}^{0n}) \right] dV, \quad (3)$$

where

$$f(Q_1, Q_2) = \frac{a(T - T_C)}{2}(Q_1^2 + Q_2^2) - \frac{b}{4}(Q_1^4 + Q_2^4) + \frac{c}{6}(Q_1^2 + Q_2^2)^3. \quad (4)$$

In this formula, a, b, and c are normal Landau coefficients calculated from the transition latent heat. κ is the gradient-energy coefficient obtained from interfacial energy of 50 mJ/m^3. C_{ijkl} is the elastic constant which is assumed to be homogeneous inside the VO_2 MBs. Lacking of experiment data, our elastic constant for VO_2 came from first principles

calculation [30]. The system is constructed by a substrate at the bottom, a thin film layer in the middle, and a gas phase on the top. For the substrate, we assumed the elastic constant to be isotropic and converted from the Young's modulus of 70 GPa. ε_{ij}^{0n} is the transformation strain (or spontaneous strain) for the *n*-th variant of R to M1 transition. The mismatch strain was set as $\varepsilon_{22} = 0.85\%$ along longitudinal direction, and all the other strain components were zero. An iteration method developed for an inhomogeneous system was used to obtain the elastic solution [31]. The parameters in our simulation are: $a = 2.98\times10^{6}$ J/m^3, $b = 2.06\times10^{8}$ J/m^3, $c = 3.35\times10^{8}$ J/m^3, $\kappa = 5.2\times10^{-12}$ J/m, substrate Young's modulus = 70GPa, substrate Poisson ratio = 0.3, C_{11} = 492 GPa, C_{22} = 407 GPa, C_{44} = 125 GPa, C_{55} = 50 GPa, C_{12} = 161 GPa, C_{13} = 32 GPa. The system starts with $(001)_R$ oriented M_1 twins at room temperature. After relaxation at 79^{o}C, 10 ^{o}C higher than the transition temperature, the equilibrium domain structures clearly show two R domains preferentially nucleating at the twin M_1 twin walls, as illustrated in Fig.5. The domain edges make angles of about ± 65^o or 90^{o}C to the c_R direction, consistent with the experimental data. Without these twin walls, the phase transition would rely on point defects to nucleate the new phase, which would result in a high degree of supersaturation.

IV. SUMMARY

In conclusion, we show that in the metal-insulator phase transition in VO_2, two distinct types of structural defects dictate the phase transition kinetics, resulting in a large kinetic asymmetry of the transition. Extended twin walls serve as a catalyst to dynamically and sustainably nucleate the metal phase and thus effectively eliminates superheating, whereas such benefit is absent in the supercooling. Localized point defects nucleate the new phase in the cooling process but much less effectively than the twin

walls. This is expected to be a general effect in first-order electronic transitions involving structural changes, as both twin walls and point defects exist ubiquitously in single crystals and epitaxial films of a vast majority of materials. In addition, unlike grain boundaries which are a result of growth, twin walls could be created, displaced and erased by post-growth processing such as heating or applying external stress [11, 32]; point defects may also be introduced by irradiation and removed by thermal annealing. Therefore, these structural defects potentially offer a new route to control the kinetics, not merely the thermodynamics, of electronic phase transitions. It can be envisioned that a metal or insulator domain can be preferentially and dynamically nucleated and eliminated at specific locations by controlling the twin wall formation or injecting point defects.

ACKNOWLEDGEMENTS

This work was supported by the Laboratory Directed Research and Development Program of Lawrence Berkeley National Laboratory (LBNL) under U.S. Department of Energy Contract No. DE-AC02-05CH11231 [irradiation and measurements], and by the National Science Foundation (NSF) under Grant No. EEC-0832819 [material synthesis and device fabrication], and NSF DMR-0820404 [theory and modelling]. We gratefully acknowledge discussion with Profs. D. Cobden and J. W. Morris. J. S. acknowledges support from the Alexander von Humboldt foundation.

REFERENCES

[1] M. Iwamatsu, J. Phys. Condens. Matter. **11**, L1 (1999).

[2] O. Mishima and H. E. Stanley, Nature **396**, 329 (1998).

[3] R. A. Aliev and V. A. Klimov, Physics of the Solid State **46**, 532 (2004).

[4] J. Wei, Z. Wang, W. Chen, and D. H. Cobden, Nature Nanotech. **4**, 420 (2009).

[5] D. Kumar, K. P. Rajeev, J. A. Alonso, and M. J. Martinez-Lope, J. Phys. Condens. Matter. **21**, 185402 (2009).

[6] M. K. Chattopadhyay, S. B. Roy, A. K. Nigam, K. J. S. Sokhey, and P. Chaddah, Phys. Rev. B **68**, 174404 (2003).

[7] A. Haldar, N. K. Singh, Y. Mudryk, K. G. Suresh, A. K. Nigam, and V. K. Pecharsky, Sol. Stat. Commun. **150**, 879 (2010).

[8] T. Ito, H. Takagi, and T. Asano, Chem. Mater. **21**, 3376 (2009).

[9] E. K. H. Salje, *Phase transitions in ferroelastic and co-elastic crystals* (Cambridge University Press, Cambridge, 1990).

[10] A. Tselev, V. Meunier, E. Strelcov, W. A. Shelton, I. A. Lukyanchuk, K. Jones, R. Proksch, A. Kolmakov, and S. V. Kalinin, ACS Nano. **4**, 4412 (2010).

[11] A. Tselev, E. Strelcov, I. A. Lukyanchuk, J. D. Budai, J. Z. Tischler, I. N. Ivanov, K. Jones, R. Proksch, S. V. Kalinin, and A. Kolmakov, Nano Lett. **10**, 2003 (2010).

[12] J. Wu, Q. Gu, B. S. Guiton, N. de Leon, O. Lian, and H. Park, Nano Lett. **6**, 2313 (2006).

[13] M. M. Qazilbash, M. Brehm, B. G. Chae, P. C. Ho, G. O. Andreev, B. J. Kim, S. J. Yun, A. V. Balatsky, M. B. Maple, F. Keilmann, et al., Science **318**, 1750 (2007).

[14] V. Eyert, Ann. Phys.-Berlin **11**, 650 (2002).

[15] M. Marezio, B. McWhan, P. D. Dernier, and J. P. Remeika, Phys. Rev. B **5**, 2541 (1972).

[16] J. C. Rakotoniaina, R. Mokranitamellin, J. R. Gavarri, G. Vacquier, A. Casalot, and G. Calvarin, J. Solid State Chem. **103**, 81 (1993).

[17] J. P. Pouget, H. Launois, J. P. D'Haenens, P. Merenda, and T. M. Rice, Phys. Rev. Lett. **35**, 873 (1975).

[18] J. Cao, E. Ertekin, V. Srinivasan, W. Fan, S. Huang, H. Zheng, J. W. L. Yim, D. R. Khanal, D. F. Ogletree, J. C. Grossman, et al., Nature Nanotech. (cover highlight) **4**, 732~737 (2009).

[19] S. Zhang, J. Y. Chou, and L. J. Lauhon, Nano Lett. **9**, 4527 (2009).

[20] J. Cao, Y. Gu, W. Fan, L. Q. Chen, C. Barrett, J. Seidel, K. Chen, N. Tamura, M. Kunz, and J. Wu, Nano Lett. **10**, 2667~2673 (2010).

[21] B. S. Guiton, Q. Gu, A. L. Prieto, M. S. Gudiksen, and H. Park, J. Am. Chem. Soc. **127**, 498 (2005).

[22] J. Cao, W. Fan, H. Zheng, and J. Wu, Nano Lett. **9**, 4001 (2009).

[23] A. Sharoni, J. G. Ramirez, and I. K. Schuller, Phys. Rev. Lett. **101**, 026404 (2008).

[24] A. L. Roytburd, J. Appl. Phys. **83**, 239 (1998).

[25] R. Lopez, T. E. Haynes, L. A. Boatner, L. C. Feldman, and R. F. Haglund, Phys. Rev. B **65** (2002).

[26] C. N. Berglund and H. J. Guggenheim, Phys. Rev. **185**, 1022 (1969).

[27] S. X. Li, K. M. Yu, J. Wu, R. E. Jones, W. Walukiewicz, J. W. Ager, W. Shan, E. E. Haller, H. Lu, and W. J. Schaff, Physical Review B **71**, 161201 (2005).
[28] A. Jones, S. Berweger, J. Wei, D. H. Cobden, and M. Raschke, Nano Lett. **10**, 1574 (2010).
[29] W. Cao and L. E. Cross, Phys. Rev. B **44**, 5 (1991).
[30] Y. Gu, J. Cao, J. Wu, and L. Q. Chen, J. Appl. Phys. **108**, 083517 (2010).
[31] S. Y. Hu and L. Q. Chen, Acta Mater. **49**, 1879 (2001).
[32] E. K. H. Salje and H. Zhang, Phase Transitions **82**, 452 (2009).

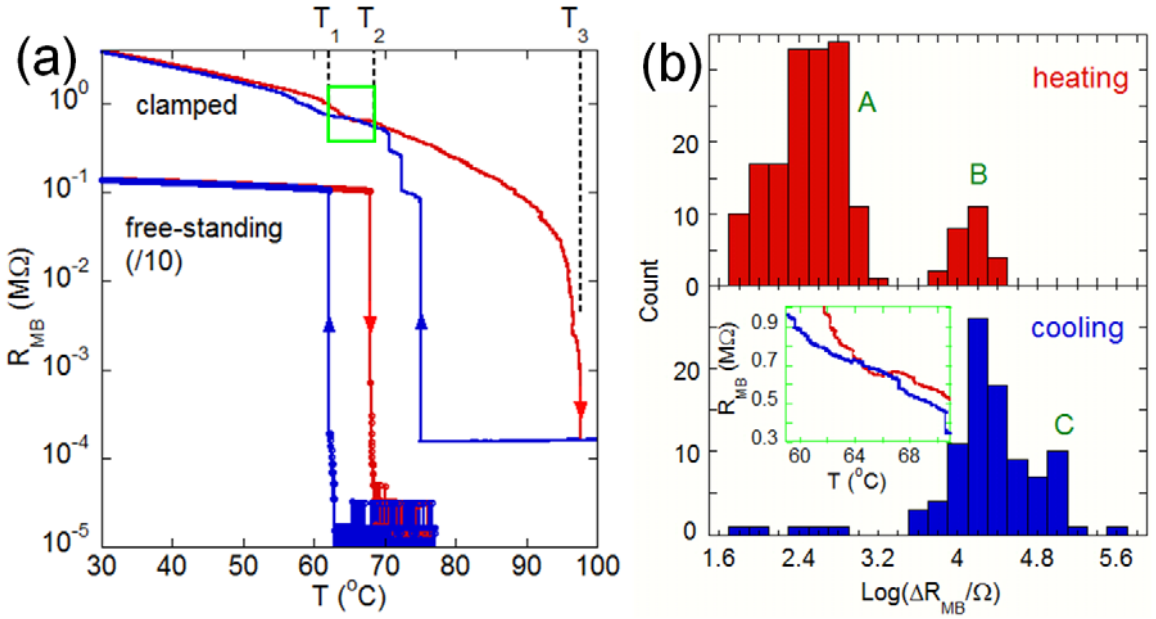

Fig. 1 Kinetic asymmetry in the metal-insulator transition of VO_2. (a) Resistance of a clamped device and a free-standing device measured at a temperature changing rate of 2°C/min. The resistance of the free-standing device is divided by 10 to add a vertical offset for clarity. (b) Distinct distribution of resistance steps on the resistance curve measured from a clamped device. Inset shows a close-up view of the boxed area on the clamped device curve in (a) where mini-steps can be seen.

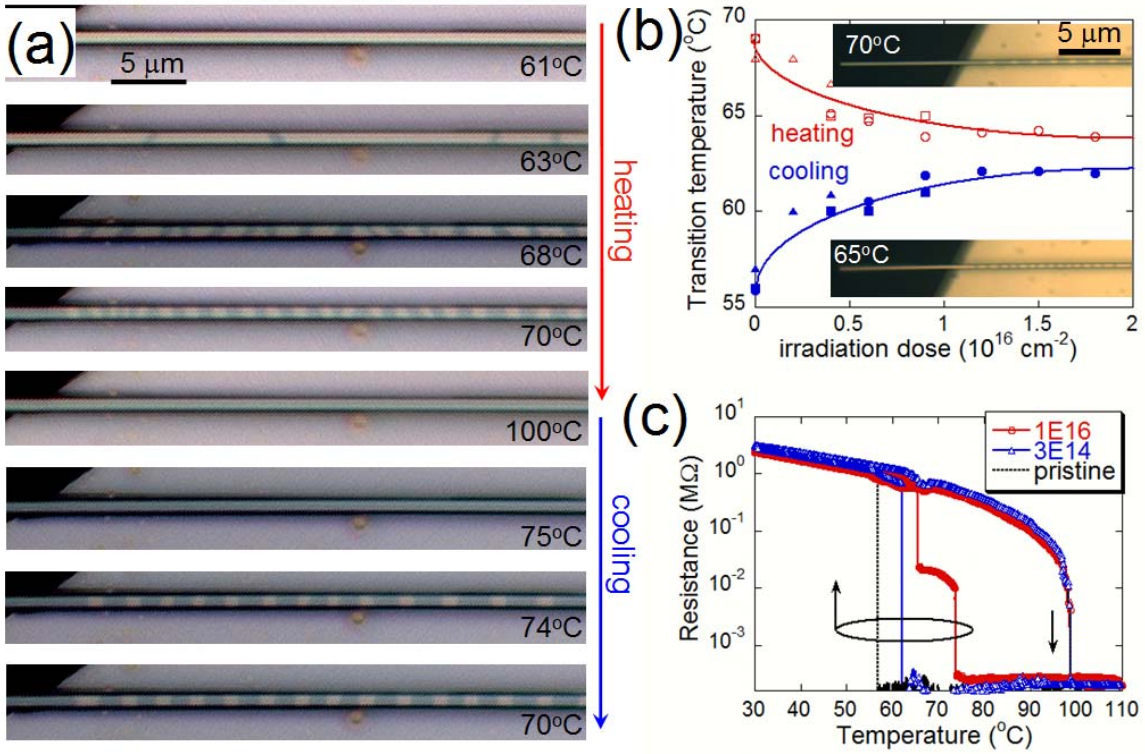

Fig. 2 (a) Optical images of an initially M_1-twinned VO_2 MB recorded during heating and cooling. M and R phases have bright and dark reflection, respectively. The left end of the MB is free-standing. Note the gradual/irregular domain formation during heating versus abrupt/regular during cooling. During cooling the M phase emerges abruptly within < 1 ^{o}C between 75 and 74 ^{o}C, and is "born periodic". (b) Optically determined transition temperatures of free-standing VO_2 as a function of 3MeV α particle irradiation dose. Different symbols represent different samples. The curves are a guide to the eye. Inset: optical image of a free standing VO_2 MB before and after the MIT. (c) Temperature-dependent four-probe resistance of a clamped device before and after two doses of α particle irradiation. The superheating is not affected yet the supercooling is clearly reduced by the irradiation.

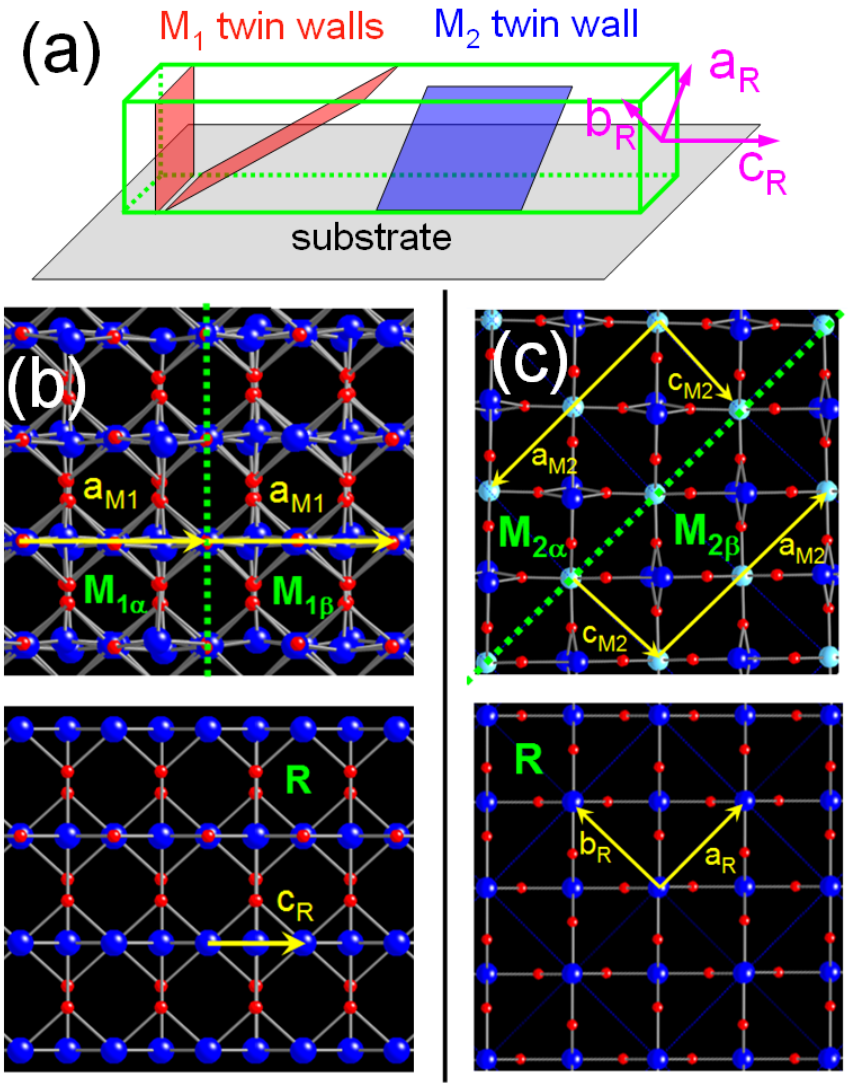

Fig. 3 The twin wall structure. (a) A schematic illustrating the orientation of 180° and 90° M_1 twin walls and of 180° M_2 twin wall along a MB. (b) Crystal structure of the 180° twin wall (green dashed line) between two variants of the M_1 phase viewed along the $\pm[011]_{M1}$ direction, and of the R phase viewed along the same direction ($[1\,\bar{1}\,0]_R$). This is the side-view direction of the MB, while the MB length is along the horizontal c_R (or a_{M1}) direction. A small angle of 0.23° exists between the a_{M1} axes of the two M_1 variants. (c) Crystal structure of the 180° twin wall (green dashed line) between two variants of the M_2 phase viewed along the $\pm b_{M2}$ direction, and of the R phase viewed along the same direction (i.e., c_R). This is the direction along the MB length. In (b) and (c), small red = O atoms, large blue and green = V atoms.

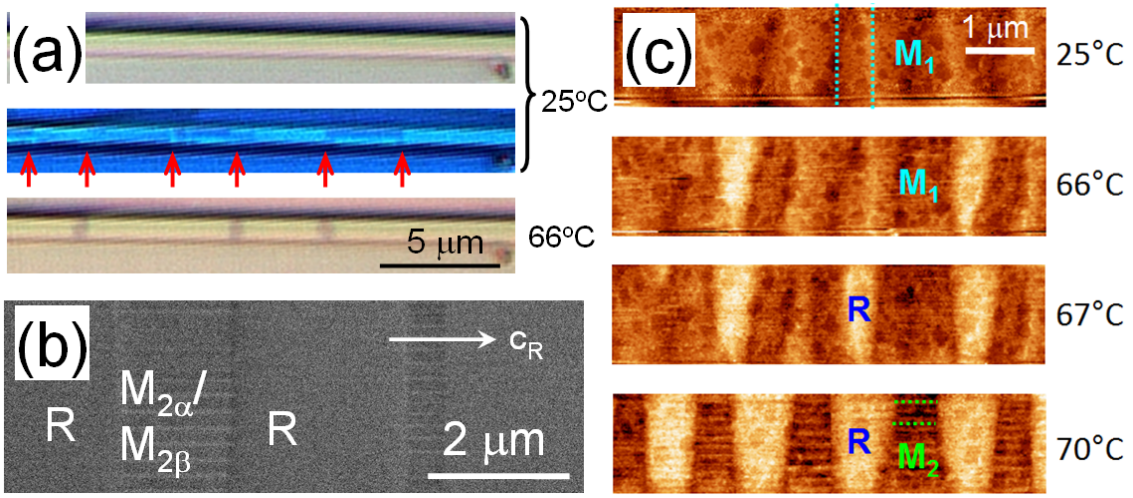

Fig. 4 The twin walls as dynamical nucleation sites for the MIT. (a) An optical image (top) and polarized image (middle) of a clamped VO_2 MB showing twinned M_1 domains with twin walls (indicated by arrows) perpendicular to MB axis, and the nucleation of R domains at some of the twin walls upon heating (bottom). (b) SEM images showing twinned M_2 domains among R domains in a clamped VO_2 beam at 70°C with M_2 twin walls parallel to the MB axis. (c) Tapping-mode AFM topography images showing $M_{1\alpha}/M_{1\beta}$ twin walls at room temperature. At higher temperatures R domains nucleate at some of the M_1 twin walls. When the R domains are sufficiently large, they induce twinned M_2 phase in the neighborhood whose twin walls in turn mediate the growth of the R phase. Some of the M_1 twin walls are highlighted by vertical dashed lines in the top image, and some of the M_2 twin walls by horizontal dashed lines in the bottom image. The c_R axis is horizontal. Note that R phase has larger height than both M_1 and M_2 phases.

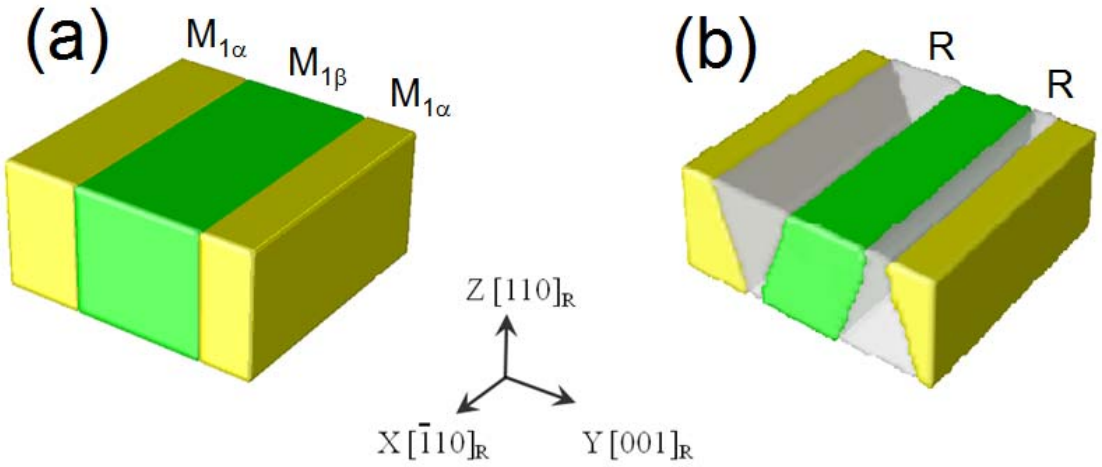

Fig. 5 Phase field modeled domains of bottom constrained VO_2. (a) $(001)_R$ twins of M_1 phase at 25°C. (b) Domain structures after relaxation at 79°C. The M_1 domain edges make an angle of about 65° with the c_R direction. The yellow and green colors represent two variants of M_1 phase. The semi-transparent part represent R phase.